A Data-Driven Model Reference Approach to Design Controllers for Power Converters via Convex Optimization

Achille Nicoletti[1] and Michele Martino[1] and Alireza Karimi[2]

***Abstract*— A new model reference data-driven approach is presented for synthesizing controllers for the CERN power converter control system. This method uses the frequency response function (FRF) of a system in order to avoid the problem of unmodeled dynamics associated with low-order parametric models. For this particular application, it is shown that a convex optimization problem can be formulated (in either the H_∞ or H_2 sense) to shape the closed-loop FRF while guaranteeing the closed-loop stability. This optimization problem is realized by linearizing a non-convex constraint around a stabilizing operating point. The effectiveness of the method is illustrated by designing a controller for the SATURN power converter which is used in the Large Hadron Collider, in injector machines, and for pulsed applications at CERN. Experimental validation in the frequency-domain is also presented.**

I. Introduction

Today's industrial processes pose challenging problems to control engineers due to the increasing complexities of system structures. In order to simplify the controller design process, these systems are approximated with low-order parameteric models; this reduces both time and effort in synthesizing a controller. However, this approximation can create stability and performance problems since these low-order models are subject to model uncertainty. Data-driven control methods seek to alleviate this problem by synthesizing controllers based on time-domain or frequency-domain data (i.e., synthesis is model independant). A survey on the differences associated with model-based control and data-driven control has been addressed in [1] and [2]; the authors assert that model-based control methods are inherently less robust due to the unmodeled dynamics of a process, and that these controllers are unsafe for practical applications. In other words, the parametric uncertainties and the unmodeled dynamics associated with the data-driven scheme are irrelevant, and the only source of uncertainty is the measurement error.

Frequency-domain based controller synthesis methods are design schemes that continue to spark the interest of many researchers. The authors in [3] establish a robust frequency-domain controller design method that requires a solution to a non-linear optimization problem. A frequency-domain loop-shaping method for fixed-structure controllers is proposed in [4]; however, stability is not guaranteed with this method and must be verified a posteriori. Controller synthesis methods belonging to the $\mathcal{H}_\infty$ control framework minimizes the $\mathcal{H}_\infty$ norm of a weighted closed-loop sensitivity function. A convex optimization approach is used to design linearly-parameterized (LP) controllers with loop-shaping and $\mathcal{H}_\infty$ performance in [5]. A frequency-domain approach for computing low-order multivariable LP controllers is presented in [6]. The $\mathcal{H}_\infty$ constraints are convexified around an initial stabilizing controller. An iterative algorithm is used that converges to a local optimal solution of the non-convex problem. However, in [7], a convex-concave approximation of the $\mathcal{H}_\infty$ constraint is used which is based on an initial stabilizing controller. More recent works that implement an iterative loop-shaping method that ensures $\mathcal{H}_\infty$ performance have been devised in [8] and [9]. These methods use the concepts from [10] to linearize non-convex constraints around an operating point. Recently, the necessary and sufficient conditions for the existence of $\mathcal{H}_\infty$ controllers for SISO systems represented by their frequency response has been proposed in [11].

The method proposed in this paper is an extension of [9] and [10] and invokes a new data-driven control design scheme for specific power converter applications at CERN. Currently, the load (i.e., the magnet of the particle accelerator) is approximated as a simple first-order system (series RL circuit); however, it has been shown in [12], [13] and [14] that the vacuum chamber of the magnet is also frequency dependent (mainly due to the coupling effects of the beam and deformations in the chamber geometry). In fact, the authors in [13] assert that even small deformations in the beam pipe can drastically change the impedance of the system and create stability issues. Therefore, it is appropriate to consider a data-driven based design to regulate the power converter control system. In this work, it is shown that a model reference design in the $\mathcal{H}_\infty$ or $\mathcal{H}_2$ sense can be formulated through a convex optimization problem; however, the methods described in this paper can also be applied to mixed $\mathcal{H}_2$ and $\mathcal{H}_\infty$ problems (i.e., minimizing the norm of weighted sensitivity functions). Additionally, with certain trivial conditions on the controller parameters, it is shown that the closed-loop stability is guaranteed.

The paper is organized as follows. The class of models represented by FRF's are addressed in section II. Section III discusses the framework of the power converter control system and its functionality at CERN. The main results and theoretical bases are addressed in section IV; in this section, loop-shaping constraints are formulated for the power con-

*This work was not supported by any organization

[1]Achille Nicoletti and Michele Martino are both with the European Organization for Nuclear Research (CERN), CH-1211 Geneva 23, Switzerland e-mail: achille.nicoletti@cern.ch / michele.martino@cern.ch

[2]Alireza Karimi is with Ecole Polytechnique Fédérale de Lausanne (EPFL), Institute of Mechanical Engineering (IGM), CH-1015 Lausanne, Switzerland e-mail: alireza.karimi@epfl.ch

verter control system. Section V is dedicated to a case study where the effectiveness of the method is demonstrated by applying the proposed design scheme to a power converter control system for a specific accelerator requirement. Finally, the concluding remarks are given in section VI.

II. Preliminaries

The class of systems discussed in this paper will be Linear Time-Invariant Single-Input Single-Output (LTI-SISO) systems that will be represented by a FRF $G(j\omega)$. The FRF can be obtained directly with a given transfer function (TF) model, or through an identification experiment using the Fourier analysis method. Let $U(j\omega)$ and $Y(j\omega)$ represent the FRFs of the system input and output signals, respectively. Then the FRF of the system can be represented as

$$G(j\omega) = Y(j\omega)U^{-1}(j\omega) \tag{1}$$

In general, a set $\mathcal{G}$ can be formulated to represent a plant model containing p FRF models:

$$\mathcal{G} = \{G_l(j\omega); \quad l = 1, \ldots, p; \quad \forall \omega \in \Omega\} \tag{2}$$

$\Omega \in [0, \infty)$. For simplicity, one model from the set $\mathcal{G}$ will be considered, and the subscript l will be omitted. However, in general, the design procedures outlined in this paper can be applied to the multi-model case (as will be seen in the case study).

Additionally, for notation purposes, let us define $\mathscr{S}$ as the set of all strictly proper (stable) TF's and $\mathscr{P}$ as the set of all proper (stable) TF's.

Remark. *In this work, the control structure will contain both discrete-time and continuous time systems. However, the proposed method synthesizes controllers based on the FRF of the system (i.e., the design method is not based on the parametric model); therefore, if the Nyquist-Shannon sampling rate is met, then the FRF of discrete-time systems will be nearly identical to that of the continuous-time system.*

III. System Framework

A schematic of the power converter control system is shown in Fig. 1. Specific portions of the schematic are color-coded in order to construct the associated block diagram. Note that there are two power converter branches assembled in series in this schematic; however, both branches possess the same components with identical values. Therefore, the analysis and control strategy can be performed in one branch and then scale the controller parameters accordingly (i.e., by a factor of 2). The input voltage for one of the high frequency (HF) filters will be denoted as v_i while the output voltage of the filter (for one branch) will be denoted as v_0. The TF from v_i to v_0 describes the output filter of the power converter for one branch. For general applications at CERN, the objective is to control the current in the magnet such that the error between this output current and a delayed version of the reference current is minimized. However, the objective of this paper is to design and implement a controller to shape the FRF between the reference voltage and v_0. This intermediate control is performed due to the fact that the output typically possesses large resonances, and a controller is required to attenuate these resonances in order to ensure better performance in the current loop. These large resonances are present because the values of the filter resistances are small (in order to reduce the power losses). Large resistance values can attenuate the resonances at the price of larger power losses. Another reason for implementing this type of control structure at CERN is for commissioning purposes; if/when faults occur in the system, each loop can be verified one at a time to ensure quality operation.

The block diagram of the control strategy is shown in Fig. 2. This block diagram is color-coded to correlate with the structure of the schematic in Fig. 1. The analog-to-digital converter (ADC) is used to process the information from the analog system to the DSP; $G_0(s)$ represents the TF from v_i to v_0; $H(s)$ represents the TF from v_0 to i_c (the current through the capacitor in the HF filter); $P_1(s)$ and $P_2(s)$ are sensors (i.e., low-pass filters); k_i and k_u are the control variable gains; $\tau\,[s]$ is an actuation delay that is used to approximate the dynamics of the power electronics; and $C(s)$ is a PI controller, i.e.,

$$C(z^{-1}) = k_{p_1} + k_{p_2}\frac{t_s z^{-1}}{1 - z^{-1}}$$

where $t_s\,[s]$ is the sampling rate of the DSP. The transfer function analyzer (TFA) is used for identification purposes, and will be discussed in the case study. As stated in the Remark in the previous section, the FRFs of continuous-time and discrete-time systems are nearly identical when the Nyquist-Shannon sampling theorem is met. Since the proposed method invokes a data-driven method using the FRF of a system, all functions discussed hereafter will be FRFs with the variable s and z^{-1} omitted from expressions.

From this framework, it can be observed that the inner feedback loops are reminiscent of a state-feedback control architecture. For this application, note that $\{G_0, P_1, P_2\} \in \mathscr{S}$ and $H \in \mathscr{P}$ (where H possesses a zero at zero). The objective of this application is to design controllers such that the FRFs from v_d to v_0 and v_r to v_0 both achieve the desired reference models.

In order to simplify the system framework, let us define the following quantities:

$$\begin{aligned} k_{m_1} &:= k_{p_1}(1 + k_u); & k_{m_2} &:= k_{p_2}(1 + k_u) \\ H_1(k) &:= k_i P_1 H; & H_2(k) &:= k_u P_2 \\ G &:= G_0 e^{-j\omega\tau}; & C_m(k) &:= k_{m_1} + k_{m_2}\frac{t_s e^{-j\omega}}{1 - e^{-j\omega}} \end{aligned} \tag{3}$$

where $k = [k_i, k_u, k_{m_1}, k_{m_2}]$. Let the FRF from v_d to v_0 be denoted as $T'(k)$ and the FRF from v_r to v_0 be denoted as $T(k)$. These closed-loop FRFs can easily be derived as follows:

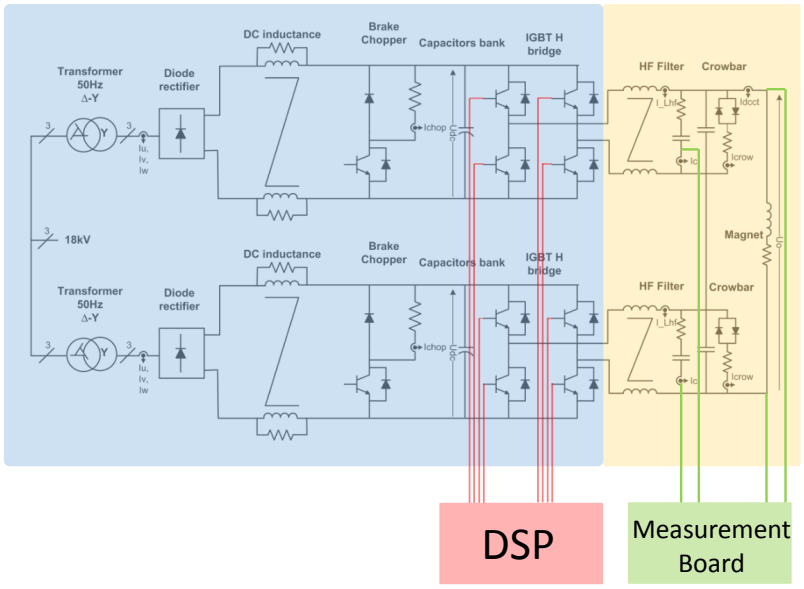

Fig. 1. Power converter control system schematic. The magnet represents the load of the process while the DSP implements the control strategy. The blue portion represents the power electronics of the converter; the yellow portion represents the analog process of the converter with the load; the red portion represents the digital-signal processor (DSP) which implements the control strategy; and the green block represents the measurement board which reads the desired control variables and sends the information to the DSP for processing.

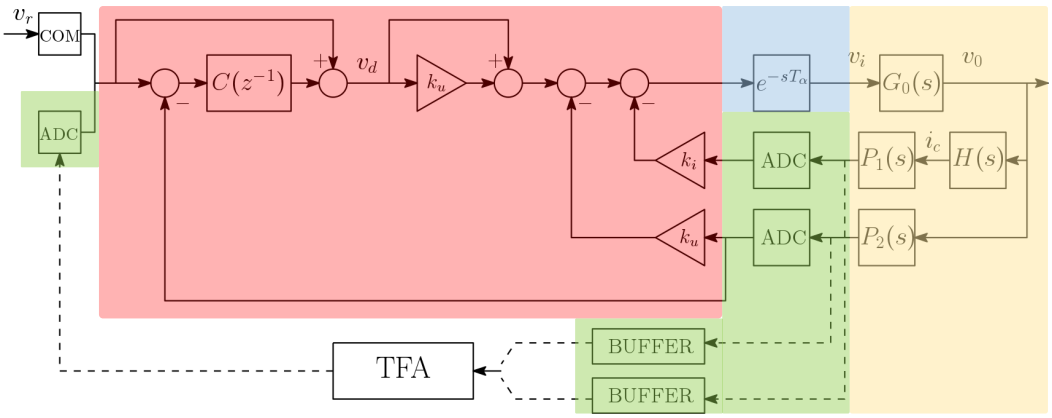

Fig. 2. Interconnection of the power converter control system. During normal operation, the TFA along with the connections indicated with a dashed-black line are not present.

$$T'(k) = \frac{G(1+k_u)}{1+G[H_1(k)+H_2(k)]} \tag{4}$$

$$T(k) = \frac{G[1+k_u+C_m(k)]}{1+G[H_1(k)+H_2(k)+P_2C_m(k)]} \tag{5}$$

For the remaining theoretical portions of this document, the loop-shaping technique will only be shown for $T(k)$, since the same procedures can also be applied to $T'(k)$.

IV. Main Results

In this section, it will be demonstrated that the performance specification of the control problem will be achieved by formulating a convex optimization problem. The controllers will be synthesized by only considering the FRF of the system.

A. Convex Approximation

The type of optimization problem that will be considered will have the following form:

$$\begin{aligned} \underset{k}{\text{minimize}} \quad & \gamma \\ \text{subject to:} \quad & y(k) - z(k) < \gamma \end{aligned} \tag{6}$$

where $y(k)$ and $z(k)$ are both convex functions of k and $\{\gamma \in \mathbb{R} : \gamma > 0\}$. This type of problem is convex-concave (due to the $-z(k)$ term); one solution to convexify this problem is to linearize $z(k)$ around an operating point k_0 and obtain the following optimization problem:

$$\begin{aligned} \underset{k}{\text{minimize}} \quad & \gamma \\ \text{subject to:} \quad & y(k) - \left[\nabla z(k_0)\right]^\top (k - k_0) < \gamma \end{aligned} \tag{7}$$

where $\nabla z(k_0)$ is the gradient of $z(k)$ evaluated at k_0.

The control methodology is based on minimizing a control objective in the $\mathcal{H}_\infty$ or $\mathcal{H}_2$ sense. In subsequent sections, it will be shown that these performance constraints will have the following quadratic form:

$$y^\star(k)\gamma^{-1}y(k) - z^\star(k)z(k) < 0 \tag{8}$$

where $y(k)$ and $z(k)$ are complex functions of the decision variable k and $(\cdot)^\star$ denotes the complex conjugate of the argument. To convexify this constraint, the term $z^\star(k)z(k)$ can be linearized around an operating point k_0; without loss of generality, it can be shown that the linearization of $z^\star(k)z(k)$ leads to the following constraint:

$$z^\star(k)z(k) \geq z^\star(k)z_0 + z(k)z_0^\star - z_0^\star z_0 \tag{9}$$

where $z_0 = z(k_0)$. The condition in (9) can easily be established by realizing the following inequality:

$$[z(k) - z_0]^\star [z(k) - z_0] \geq 0 \tag{10}$$

With this linearization, a sufficient condition for the inequality in (8) can be developed as follows:

$$y^\star(k)\gamma^{-1}y(k) - [z^\star(k)z_0 + z(k)z_0^\star - z_0^\star z_0] < 0 \tag{11}$$

By using the Shur Complement Lemma [15], the above condition can be expressed in terms of a Linear-Matrix-Inequality (LMI):

$$\begin{bmatrix} z^\star(k)z_0 + z(k)z_0^\star - z_0^\star z_0 & y^\star(k) \\ y(k) & \gamma \end{bmatrix} \succ 0 \tag{12}$$

This type of formulation will be used in section IV-C in order to construct a model reference control objective.

B. Control Performance

For SISO systems, and for a stable system $X(s)$, the $\mathcal{H}_2$ and $\mathcal{H}_\infty$ norms are defined as follows:

$$\|X\|_2^2 := \frac{1}{2\pi}\int_{-\infty}^{\infty} |X(j\omega)|^2 d\omega$$
$$\|X\|_\infty := \sup_\omega |X(j\omega)|$$

It is imperative to note that the boundedness of spectral norm X does not guarantee the stability of X.

A model reference criterion can be considered as a form of control performance. If T is the closed-loop FRF and T_d is the desired FRF, then one can consider minimizing $(T - T_d)$ in either the $\mathcal{H}_2$ or $\mathcal{H}_\infty$ sense in order to shape T. The next section will discuss how such an optimization problem can be formulated for this type of control methodology.

C. Model Reference Design

As asserted in section III, the objective of this control problem is to shape the FRF of $T(k)$. Suppose that a desired loop-shape is specified as T_d; the objective is to design the controllers in k such that the closed-loop system $T(k)$ coincides with T_d in the $\mathcal{H}_\infty$ or $\mathcal{H}_2$ sense. In the $\mathcal{H}_\infty$ sense, the objective is to minimize $\|T(k) - T_d\|_\infty$; an equivalent representation of this objective is to minimize γ such that $\|T(k) - T_d\|_\infty < \gamma$. This criterion is satisfied if the the following optimization problem is considered:

$$\begin{aligned} \underset{k\in\mathbb{R}}{\text{minimize}} \quad & \gamma \\ \text{subject to:} \quad & \left[T(k) - T_d\right]^\star \left[T(k) - T_d\right] < \gamma \end{aligned} \tag{13}$$

for all $\omega \in \Omega$. It can be observed that the constraint in (13) is not convex. Let us now define the following quantities:

$$\begin{aligned} w(k) &= G[1 + k_u + C_m(k)] \\ z(k) &= 1 + G[H_1(k) + H_2(k) + P_2 C_m(k)] \end{aligned} \tag{14}$$

where it is evident that $T(k) = w(k)z^{-1}(k)$; then the constraint in (13) can be written as:

$$\left[w(k) - z(k)T_d\right]^\star \gamma^{-1} \left[w(k) - z(k)T_d\right] - z^\star(k)z(k) < 0 \tag{15}$$

Note that this constraint has the exact form as in (8); therefore, the convex constraint in (12) can be utilized to construct the model-reference optimization problem as follows:

$$\begin{aligned} \underset{k\in\mathbb{R}}{\text{minimize}} \quad & \gamma \\ \text{subject to:} \quad & \\ & \begin{bmatrix} z^\star(k)z_0 + z_0^\star z(k) - z_0^\star z_0 & [w(k) - z(k)T_d]^\star \\ w(k) - z(k)T_d & \gamma \end{bmatrix} \succ 0 \end{aligned} \tag{16}$$

for all $\omega \in \Omega$, where $z_0 = 1 + G[H_1(k_0) + H_2(k_0) + P_2 C_m(k_0)]$ and $k_0 = [k_{i,0}, k_{u,0}, k_{m_1,0}, k_{m_2,0}]$ are the initializing gains. In a similar manner, the following convex optimization problem can be considered for minimizing $\|T(k) - T_d\|_2^2$, as follows:

$$\begin{aligned} \underset{k\in\mathbb{R}}{\text{minimize}} \quad & \int_0^\infty \gamma(\omega) d\omega \\ \text{subject to:} \quad & \\ & \begin{bmatrix} z^\star(k)z_0 + z_0^\star z(k) - z_0^\star z_0 & [w(k) - z(k)T_d]^\star \\ w(k) - z(k)T_d & \gamma(\omega) \end{bmatrix} \succ 0 \end{aligned} \tag{17}$$

for all $\omega \in \Omega$. For this $\mathcal{H}_2$ problem, note that γ is now a function of ω (which contrasts with the optimization problem in the $\mathcal{H}_\infty$ sense).

Remark. *Note that the choice of the initializing gains in k_0 may affect the stability of the closed-loop system (for either the optimization problems concerning the $\mathcal{H}_\infty$ or $\mathcal{H}_2$ norms). The next section will discuss how to select these gains in order to ensure stability.*

D. Stability Analysis

The loop-shaping constraints developed in the previous section do not guarantee the stability of the closed-loop system. Setting a desired FRF to shape a closed-loop FRF is analogous to bounding the closed-loop FRF; it can be shown that unstable systems can still possess bounded FRF's.

The initializing controllers in k_0 play an important role in guaranteeing the stability of the closed-loop system. By using the Nyquist criterion, the stability of the closed-loop system can be ensured if certain conditions are met for these initializing gains. In this paper, it is assumed that the Nyquist contour has some small detours around the poles of the open-loop system on the imaginary axis.

The following properties will be needed in order to properly analyze the stability conditions of the system:

Definition 1. *Let* $\text{wno}\{A(s)\}$ *refer to the winding number; in the counterclockwise sense,* $\text{wno}\{A(s)\}$ *represents the image of $A(s)$ around the origin when s traverses the Nyquist contour (with small detours around the poles of $A(s)$ on the imaginary axis). Then the following properties hold:*

$$\text{wno}\big\{A_1(s)A_2(s)\big\} = \text{wno}\big\{A_1(s)\big\} + \text{wno}\big\{A_2(s)\big\} \quad (18)$$

$$\text{wno}\big\{A(s)\big\} = -\text{wno}\big\{A^\star(s)\big\} \quad (19)$$

$$\text{wno}\big\{A(s)\big\} = -\text{wno}\big\{A^{-1}(s)\big\} \quad (20)$$

The open-loop FRF of the system $T(k)$ in Fig. 2 is given as

$$L(k) = G[H_1(k) + H_2(k) + P_2C_m(k)].$$

Let $F(k) = H_1(k) + H_2(k) + P_2C_m(k)$ such that $L(k) = GF(k)$; by the Nyquist stability criterion, the closed-loop system is stable if and only if $1 + GF$ makes $n_G + n_F$ counter-clockwise encirclements of the origin (where n_G and n_F are, respectively, the number of right-half plane (RHP) poles of G and F). The Nyquist plot of $1 + GF$ must also not pass through the origin.

Theorem 1. *Suppose that k_i, k_u, k_{m_1}, and k_{m_2} are feasible solutions to the following constraint:*

$$\begin{aligned} z^\star(k)z_0 + z_0^\star z(k) > 0 \\ \forall \omega \in \Omega \end{aligned} \quad (21)$$

where

$$\begin{aligned} z(k) &= 1 + G[H_1(k) + H_2(k) + P_2C_m(k)] \\ z_0 &= 1 + G[H_1(k_0) + H_2(k_0) + P_2C_m(k_0)] \end{aligned}$$

with $\{G, H_1, H_2\} \in \mathscr{S}$. Then the closed-loop system T is stable if the parameters in the set k_0 are stabilizing initial gains.

Proof: The proof is based on the Nyquist stability criterion and the properties of the winding number. The winding number of $z^\star(k)z_0$ is given as follows:

$$\begin{aligned} \text{wno}\{z^\star(k)z_0\} &= \text{wno}\{z^\star\} + \text{wno}\{z_0\} \\ &= -\text{wno}\{1 + GF(k)\} \\ &\quad + \text{wno}\{1 + GF(k_0)\} \end{aligned} \quad (22)$$

where $F(k_0) = H_1(k_0) + H_2(k_0) + C_m(k_0)$. Note that $F(k)$ is strictly proper and $GF(k)$ is strictly proper; therefore, the winding number of $z^\star(k)z_0$ can be evaluated over Ω instead of the D-contour. Additionally, the constraint in (21) implies that $\Re\{z^\star(k)z_0\} > 0$ (where $\Re\{\cdot\}$ indicates the real part of the argument), which signifies that the Nyquist plot of $z^\star(k)z_0$ will not pass through or encircle the origin. Therefore, $\text{wno}\{z^\star(k)z_0\} = 0$; from (22), the following condition can then be realized:

$$\text{wno}\{1 + GF(k)\} = \text{wno}\{1 + GF(k_0)\} \quad (23)$$

The condition in (23) implies that if the initializing controllers k_0 are stabilizing (i.e., the open-loop system $GF(k_0)$ meets the Nyquist stability criterion), then the closed-loop system will be stable. ■

E. Initializing Controller

For the given structure in Figure. 2, it remains to be shown how to select the initial stabilizing controllers in order to guarantee the stability of the closed-loop system. From the control structure of the power converter control system, it can be observed that if all the controller gains in Figure. 2 are set to zero, then the system will be in open-loop. However, since $G \in \mathscr{S}$, then selecting $k_0 = 0$ will guarantee the stability of the closed-loop system.

F. Convex Optimization via Semi-Definite Programming

All of the optimization problems considered in section IV-C are known as semi-infinite programming (SIP) problems since there are a finite number of optimization variables k and an infinite number of constraints with respect to ω. To solve any of these problems, the optimization algorithm can be converted to a semi-definite programming (SDP) problem. In this manner, a predefined frequency grid can be implemented in order to solve a finite number of constraints. In other words, for a finite number of frequency points n selected in $\omega \in [0, \infty)$, then n constraints must be satisfied. This frequency grid can be predefined in a variety of manners (see [16], [17], [18]).

V. Case Study

The focus of this case study will be on the SATURN power converter, which incorporates the control methodology shown in Figure. 2 and uses the power converter with the architecture shown in Figure. 1. The SATURN converter is used in the Large Hardron Collider, in injector machines, in

TABLE I

SYSTEM CHARACTERISTICS OF SATURN POWER CONVERTER

	Value	Units
U_0 (Output Voltage)	700	V
I_0 (Output Current)	850	A
Input Power	18	kV
Input Frequency	50	Hz
IGBT equivalent switching frequency	5000	Hz
Transformer Weight	4500	kg
Control Type	RegFGC3 Type 10 / Ethernet [19]	–

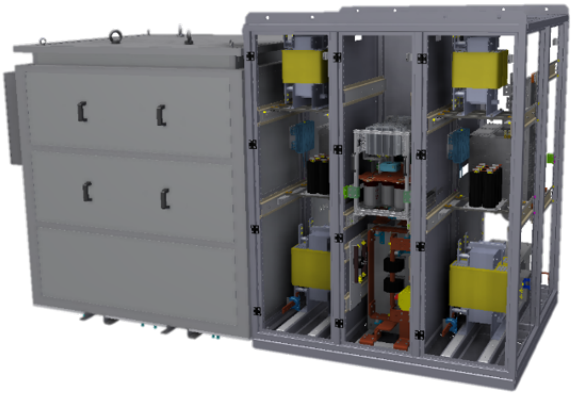

Fig. 3. SATURN power converter used for various applications at CERN.

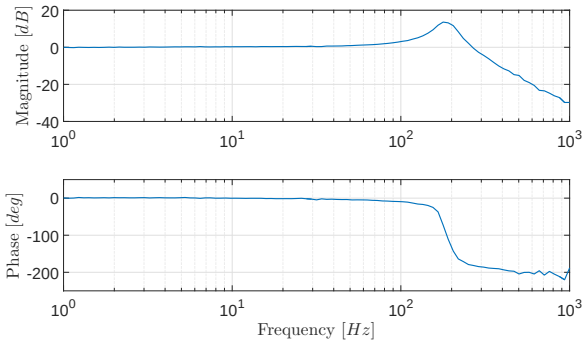

Fig. 4. Frequency response measurement of GP_2.

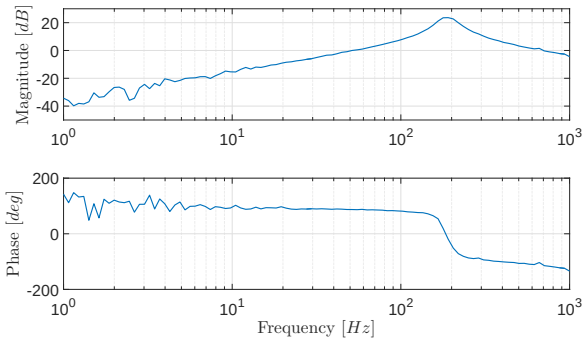

Fig. 5. Frequency response measurement of GHP_1.

experimental areas to power warm magnets, and for DC or pulsed applications. In this power converter, a $18\,kV/50\,Hz$ transformer is used with a diode rectifier and a DC-Link filter for the AC/DC conversion. An IGBT bridge (4 quadrant operation) is then used for a DC/DC conversion, and the output of this bridge is then fed into the filter. For this application, two identical modules are assembled in series (which doubles the output voltage) where the equivalent switching frequency of this bridge is $5\,kHz$. The DSP is also running at a rate of $5\,kHz$. A complete assembly of the SATURN power converter is shown in Fig. 3. Table. I displays the values of the system characteristics of this power converter.

A. Frequency Response Measurement

Since the proposed method uses a data-driven methodology with frequency-domain data, the FRF of each subsystem within the power converter control system must be obtained. In other words, we must obtain the FRF of G, H, P_1, P_2, and the ADCs. The signals that are accessible for the measurements are shown in Fig. 2, which are the outputs of the sensors P_1 and P_2 and the input of the converter control system (which goes into an ADC). Note that the ADC at the output of the TFA has very fast dynamics, and can be neglected. Therefore, when all of the controller gains are set to zero, we are able to obtain the frequency responses of GHP_1 and GP_2. However, note that G appears independently of P_2 in (4) and (5); since P_1 and P_2 are sensors with very high bandwidths relative to G (approximately $10\,kHz$), then $G \approx GP_2$ at frequencies less than $1\,kHz$. The FRF of the ADCs in the control loop are not measured since the output of these ADCs are digital signals. However, since these ADCs have very fast dynamics, they can be approximated as pure delays. Since these delays are known to be within specific ranges, a multi-model design can be formulated to incorporate this uncertainty in the design.

The frequency response of the subsystems were obtained with a transfer function analyzer (Powertek GP102) which implements a sine-sweep method that recovers the gain and phase of a system at discrete frequency points. The appropriate scaling factors were taken into account for the measurements (due to the series connection of the SATURN modules) in order to coincide with the structure used in Fig. 2. The frequency responses of GP_2 and GHP_1 are shown in Fig. 4 and Fig. 5, respectively.

B. Controller Synthesis

For this application, it was desired to shape $T'(k)$ and $T(k)$ such that a bandwidth of $300Hz$ and $500Hz$ is attained, respectively (where both achieve a damping of $\zeta = 0.8$). Note that in both of these TF's, a pure delay appears in the numerator; therefore, the performance of the loop-shape algorithm can be improved by specifying a desired loop-shape $T_d(s) = T_d^*(s)e^{-s\tau}$ where $T_d^*(s)$ was selected as a

standard second order process, i.e.,

$$T_d^*(s) = \frac{\omega_d^2}{s^2 + 2\zeta\omega_d s + \omega_d^2} \tag{24}$$

where ζ is the damping factor and

$$\omega_d = \frac{2\pi f_d}{\sqrt{1 - 2\zeta^2 + \sqrt{2 - 4\zeta^2 + 4\zeta^4}}}$$

where f_d is the desired closed-loop bandwidth. In other words, T_d is simply a delayed version of the second order process. There is some uncertainty associated with the delay τ; the range of this delay is $\tau \in [0, 200]\mu s$ with a nominal value of $100\mu s$. Therefore, for tracking purposes, $\tau = 100\mu s$ in $T_d(s)$ can be selected as a viable performance criteria. Note that selecting τ to be another value within the uncertain range will not significantly impact the response. The critical values in the desired response are f_d and ζ.

Although the delay in G was captured in the frequency response measurement, it is known that there also exists an additional measurement delay τ_e that was not captured in the identification experiment (i.e., the delay from the ADCs in the control loop). The value of the delay is uncertain and is known to be in the range of $\tau_e \in [0, 30]\mu s$. Therefore, a multi-model design can be considered where the additional delay can be gridded in this range and incorporated into the closed-loop TF's. The grid was established in intervals of $5\ \mu s$ (i.e., $\tau_{e_i} = [0, 5, \ldots 30]\mu s$, $i = 1, \ldots, 7$).

In the $\mathcal{H}_\infty$ sense, the optimization problem to consider for this case study is as follows:

$$\begin{aligned} \underset{k\in\mathbb{R}}{\text{minimize}} \quad & \gamma \\ \text{subject to:} \quad & \|T_i(k) - T_d\|_\infty < \gamma \\ & \|T_i'(k) - T_d'\|_\infty < \gamma \\ & i = 1, \ldots, 7 \end{aligned} \tag{25}$$

where $T_i(k)$ and $T_i'(k)$ are the closed-loop TF's that incorporate the additional i-th delay in τ_{e_i}; T_d is the desired closed-loop TF for shaping $T(k)$ (with a desired bandwidth of $f_d = 500\ Hz$ and damping $\zeta = 0.8$); T_d' is the desired closed-loop TF for shaping $T'(k)$ (with a desired bandwidth of $f_d' = 300\ Hz$ and damping $\zeta' = \zeta$). In the $\mathcal{H}_2$ sense, the optimization problem to consider is as follows:

$$\begin{aligned} \underset{k\in\mathbb{R}}{\text{minimize}} \quad & \int_0^\infty \gamma(\omega) d\omega \\ \text{subject to:} \quad & \|T_i(k) - T_d\|_2^2 < \gamma(\omega) \\ & \|T_i'(k) - T_d'\|_2^2 < \gamma(\omega) \\ & i = 1, \ldots, 7 \end{aligned} \tag{26}$$

These optimization problems can be transformed to convex problems by implementing the methods outlined in section IV-C.

C. Experimental Results

The constraints in the optimization problem in (25) and (26) were first converted to LMI constraints. Since the transfer function analyzer provides the gain and phase at discrete frequency points, the optimization problem then becomes an SDP problem. For solving the $\mathcal{H}_2$ problem in SDP form, the objective function in (26) must be discretized where $\int \gamma(\omega) d\omega \rightarrow \sum_i \gamma_i(\omega)$.

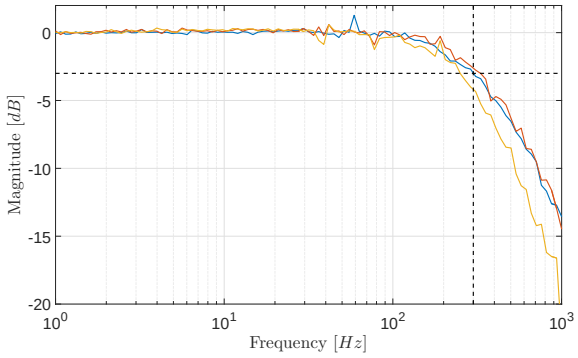

Fig. 6. The closed-loop response of $|T'|$; data-driven method with $\mathcal{H}_\infty$ performance (red line); data-driven method with $\mathcal{H}_2$ performance (blue line); model-based approach with $\mathcal{H}_2/\mathcal{H}_\infty$ performance (yellow line); $-3\ dB$ point representing $300\ Hz$ bandwidth (dashed-black line).

For comparative purposes, controllers were designed by considering the model of the process. Since there was uncertainty associated with the delay τ, a multi-model approach was implemented to ensure that the performance was attained for the uncertain values. Therefore, for the model-based design, the problem in (25) and (26) was solved by gridding in both τ and τ_e.

The closed-loop frequency response of $|T'|$ and $|T|$ are shown in Fig. 6 and Fig. 7 (respectively) for the solutions obtained by minimizing both the $\mathcal{H}_\infty$ and $\mathcal{H}_2$ norms of the process. From these figures, it can be observed that the model-based design produces the worst performance while the data-driven based design achieves the desired performance for both T and T'. The performance achieved by the data-driven method (in both the $\mathcal{H}_\infty$ and $\mathcal{H}_2$ minimization cases) are comparable.

Remark. *Note that the solutions obtained for the model-based design were nearly identical for both the $\mathcal{H}_2$ and $\mathcal{H}_\infty$ problems. Hence the single result shown for the model-based design in Fig. 6 and Fig. 7.*

Table. II displays the optimal solutions for all criteria considered in this case study. It can be observed that the optimal solutions γ^* obtained with the data-driven method are less than the solutions obtained with the model-based approach. This is due to the fact that the uncertainty in the delay τ for the model-based design was too conservative. This conservativeness was significantly reduced in the data-driven approach since the delay τ was captured in the FRF identification experiment.

VI. Conclusion

A new data-driven method for computing a controller for the CERN power converter control system that attains $\mathcal{H}_2$ or $\mathcal{H}_\infty$ performance has been presented. A frequency-domain approach has been used in order to avoid the problem

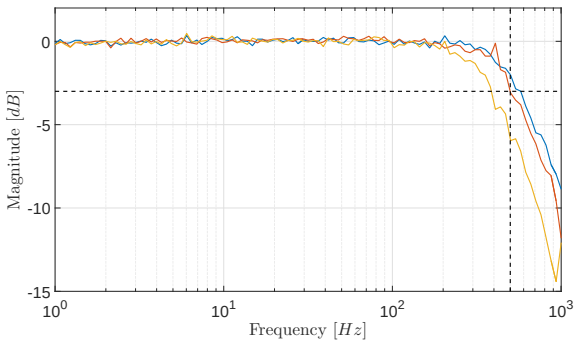

Fig. 7. The closed-loop response of $|T|$; data-driven method with $\mathcal{H}_\infty$ performance (red line); data-driven method with $\mathcal{H}_2$ performance (blue line); model-based approach with $\mathcal{H}_2/\mathcal{H}_\infty$ performance (yellow line); $-3\,dB$ point representing $500\,Hz$ bandwidth (dashed-black line).

TABLE II

COMPARISON OF OPTIMAL SOLUTIONS BETWEEN DATA-DRIVEN AND MODEL-BASED METHODOLOGY

	k_i^*	k_u^*	k_{p1}^*	k_{p2}^*	γ^*
$\mathcal{H}_\infty$ (data-driven)	1.29	3.80	0.42	$2 \cdot 10^{-6}$	0.057
$\mathcal{H}_2$ (data-driven)	1.39	3.82	0.60	$7 \cdot 10^{-7}$	0.108 (peak value)
$\mathcal{H}_\infty$ (model-based)	0.95	1.70	0.48	$3 \cdot 10^{-7}$	0.149
$\mathcal{H}_2$ (model-based)	0.95	1.70	0.48	$3 \cdot 10^{-7}$	0.191 (peak value)

of unmodeled dynamics associated with parametric models. A non-convex loop-shaping constraint was convexified by linearizing the non-convex function around a stabilizing operating point. This linearization process allowed the use of the Shur Complement Lemma to construct an LMI and solve a convex optimization problem. This method has been applied to a power converter control system which uses a specific controller structure and is used for experimental purposes at CERN. In the case study presented in this paper, it has been shown that the proposed data-driven method offers a systematic optimization-based approach that meets the challenging specifications required for the application. The experiments have confirmed that the data-driven approach significantly reduces the conservativeness associated with the modeling process. For future work, it will be desired to develop a method (in a data-driven sense) that will implement a search algorithm such that the global optimal solution to the $\mathcal{H}_\infty$ problem can be obtained.

REFERENCES

[1] Z.-S. Hou and Z. Wang, "From model-based control to data-driven control: Survey, classification and perspective," *Information Sciences*, vol. 235, pp. 3–35, 2013.

[2] S. Formentin, K. Van Heusden, and A. Karimi, "A comparison of model-based and data-driven controller tuning," *Int. Journal of Adaptive Control and Signal Processing*, 2013.

[3] S. Khadraoui, H. Nounou, M. Nounou, A. Datta, and S. Bhattacharyya, "Robust control design method for uncertain system using a set of measurements," in *American Control Conference (ACC), 2013*, 2013, pp. 4325–4330.

[4] ——, "A control design method for unknown systems using frequency domain data," in *Control Conference (ASCC), 2013 9th Asian*. IEEE, 2013, pp. 1–6.

[5] A. Karimi and G. Galdos, "Fixed-order H_∞ controller design for nonparametric models by convex optimization," *Automatica*, vol. 46, no. 8, pp. 1388–1394, 2010.

[6] M. Saeki, M. Ogawa, and N. Wada, "Low-order H_∞ controller design on the frequency domain by partial optimization," *International Journal of Robust and Nonlinear Control*, vol. 20, no. 3, pp. 323–333, 2010.

[7] M. Hast, K. J. Aström, B. Bernhardsson, and S. Boyd, "PID design by convex-concave optimization," in *European Control Conference*, Zurich, Switzerland, 2013, pp. 4460–4465.

[8] T. Usami, K. Yubai, D. Yashiro, and S. Komada, "Multivariable fixed-structural controller design for H_∞ loop shaping method by iterative LMI optimization using frequency response data," in *International Conference on Advanced Mechatronic Systems (ICAMechS)*. IEEE, 2016, pp. 218–223.

[9] A. Karimi and C. Kammer, "A data-driven approach to robust control of multivariable systems by convex optimization," *to appear in Automatica*, 2016.

[10] S. Boyd, M. Hast, and K. J. Åström, "MIMO PID tuning via iterated LMI restriction," *International Journal of Robust and Nonlinear Control*, vol. 26, no. 8, pp. 1718–1731, 2016.

[11] A. Karimi, A. Nicoletti, and Y. Zhu, "Robust H_∞ controller design using frequency-domain data via convex optimization," *available online in International Journal of Robust and Nonlinear Control*, 2016.

[12] E. Keil and B. Zotter, "The impedance of layered vacuum chambers," in *EPAC Stockholm*, 1998.

[13] C.-K. Ng and T. Weiland, "Impedance analysis of the PEP-II vacuum chamber," in *Proceedings of the Particle Accelerator Conference*, vol. 5. IEEE, 1995, pp. 3061–3063.

[14] G. Nassibian and F. Sacherer, "Methods for measuring transverse coupling impedances in circular accelerators," *Nuclear Instruments and Methods*, vol. 159, no. 1, pp. 21–27, 1979.

[15] A. Ben-Tal, L. El Ghaoui, and A. Nemirovski, *Robust optimization*. Princeton University Press, 2009.

[16] G. Galdos, A. Karimi, and R. Longchamp, "H_∞ controller design for spectral MIMO models by convex optimization," *Journal of Process Control*, vol. 20, no. 10, pp. 1175 – 1182, 2010.

[17] P. Seiler, B. Vanek, J. Bokor, and G. J. Balas, "Robust H_∞ filter design using frequency gridding," in *American Control Conference (ACC), 2011*. IEEE, 2011, pp. 1801–1806.

[18] G. Ferreres and C. Roos, "Efficient convex design of robust feedforward controllers," in *44th IEEE Conference on Decision and Control*, Seville, Spain, December 2005, pp. 6460–6465.

[19] D. Calcoen, Q. King, and P. Semanaz, "Evolution of the CERN power converter function generator/controller for operation in fast cycling accelerators," in *International Conference on Accelerator and Large Experimental Control Systems (ICALEPCS)*, Grenoble, France, 2011.